Alkanethiolate Gold Cluster Molecules with Core Diameters from 1.5 to 5.2 nm: Core and Monolayer Properties as a Function of Core Size

Michael J. Hostetler,[†] Julia E. Wingate,[†] Chuan-Jian Zhong,[‡] Jay E. Harris,[†] Richard W. Vachet,[†] Michael R. Clark,[†] J. David Londono,[§] Stephen J. Green,[†] Jennifer J. Stokes,[†] George D. Wignall,[§] Gary L. Glish,[†] Marc D. Porter,[‡] Neal D. Evans,[||] and Royce W. Murray*[,†]

Kenan Laboratories of Chemistry, University of North Carolina, Chapel Hill, North Carolina 27599-3290, Department of Chemistry, Iowa State University, Ames, Iowa 50011-3111, Oak Ridge National Laboratory, P.O. Box 2008, Oak Ridge, Tennessee 37831, and Oak Ridge Institute for Science and Education, P.O. Box 117, Oak Ridge, Tennessee 37831

Received June 5, 1997. In Final Form: October 23, 1997[⊗]

The mean size of the gold (Au) core in the synthesis of dodecanethiolate-stabilized Au cluster compounds can be finely adjusted by choice of the Au:dodecanethiolate ratio and the temperature and rate at which the reduction is conducted. The Au clusters have been examined with a large number of independent analytical tools, producing a remarkably consistent picture of these materials. Average cluster and core dimensions, as ascertained by ^{1}H NMR line broadening, high-resolution transmission electron microscopy, small-angle X-ray scattering, and thermogravimetric analysis, vary between diameters of 1.5 and 5.2 nm (∼110−4800 Au atoms/core). The electronic properties of the Au core were examined by UV/vis and X-ray photoelectron spectroscopy; the core appears to remain largely metallic in nature even at the smallest core sizes examined. The alkanethiolate monolayer stabilizing the Au core ranges with core size from ∼53 to nearly 520 ligands/core, and was probed by Fourier transform infrared spectroscopy, differential scanning calorimetry, contact-angle measurements, and thermal desorption mass spectrometry. The dodecanethiolate monolayer on small and large core clusters exhibits discernable differences; the line dividing "3-dimensional" monolayers and those resembling self-assembled monolayers on flat Au (2-dimensional monolayers) occurs at clusters with ∼4.4 nm core diameters.

The ability to selectively synthesize metal nanoparticles of any desired size or shape would generate significant opportunities in chemistry, because catalytic, optical, magnetic, and electronic activities can be dimensionally sensitive.[1−3] Very small clusters (<∼50 metal atoms) act like large molecules, whereas large ones (>∼300 atoms) exhibit characteristics of a bulk sample of those atoms. Between these extremes lie materials with intermediate chemical and physical properties that are largely unknown; gaining access to and evidence of such materials is one of the themes of this paper.

As an example, the optical properties of a metal cluster, including the intensity and energy of its surface plasmon bands, have been strongly correlated to its size.[4] The smallest clusters of some [including gold (Au)], but not all, metals exhibit electronic spectra with molecular transitions; as the number of atoms increases, over a range that depends on the particular metal in the cluster, the plasmon band intensifies until the optical spectrum resembles that of the bulk metal. Clearly, investigations of additional cluster properties over a broad range of sizes would be valuable. What is needed is the ability to selectively synthesize large quantities of these materials with ease.

In this regard, recent reports on the synthesis and characterization of relatively monodisperse Au nanoparticles are noteworthy.[5−7] These clusters of Au atoms are stabilized to a remarkable degree by a monolayer of chemisorbed alkanethiolate ligands and are readily

* Author to whom correspondence should be addressed.
[†] Kenan Laboratories of Chemistry, University of North Carolina.
[‡] Department of Chemistry, Iowa State University.
[§] Oak Ridge National Laboratory.
[||] Oak Ridge Institute for Science and Education.

[⊗] Abstract published in *Advance ACS Abstracts,* December 15, 1997.

(1) Matijević, E. *Curr. Opin. Coll. Interface Sci.* **1996**, *1*, 176−183. (b) Belloni, J. *Curr. Opin. Coll. Interface Sci.* **1996**, *1*, 184−196. (c) Klabunde, K. J.; Stark, J.; Koper, O.; Mohs, C.; Park, D. G.; Decker, S.; Jiang, Y.; Lagadic, I.; Zhang, D. *J. Phys. Chem.* **1996**, *100*, 12142−12153. (d) Haberland, H., Ed. *Clusters of Atoms and Molecules*; Springer-Verlag: New York, 1994. (e) *Clusters and Colloids. From Theory to Applications*; Schmid, G., Ed.; VCH: New York, 1994. (f) Heinglein, A. *Ber. Bunsenges Phys. Chem.* **1995**, *99*, 903−913. (g) Schmid, G. *Chem. Rev.* **1992**, *92*, 1709−1727. (h) Fendler, J. H.; Meldrum, F. C. *Adv. Mater.* **1995**, *7*, 607−632. (i) Schmid, G.; Maihack, V.; Lantermann, F.; Peschel, S. *J. Chem. Soc., Dalton Trans.* **1996**, 589−595.

(2) (a) Schon, G.; Simon, U. *Colloid Polym. Sci.* **1995**, *273*, 101−117. (b) Schon, G.; Simon, U. *Colloid Polym. Sci.* **1995**, *273*, 202−218.

(3) (a) Weller, H. *Angew. Chem., Int. Ed. Engl.* **1993**, *32*, 41−53. (b) Murray, C. B.; Kagan, C. R.; Bawendi, M. G. *Science* **1995**, *270*, 1335−1338. (c) Guzelian, A. A.; Katari, J. E. B.; Kadavanich, A. V.; Banin, U.; Hamad, K.; Juban, E.; Alivasatos, A. P.; Wolters, R. H.; Arnold, C. C.; Heath, J. R. *J. Phys. Chem.* **1996**, *100*, 7212−7219. (d) Ahmadi, T. S.; Wang, Z. L.; Henglein, A.; El-Sayed, M. A. *Chem. Mater.* **1996**, *8*, 1161−1163. (e) Ahmadi, T. S.; Wang, Z. L.; Green, T. C.; Henglein, A.; El-Sayed, M. A. *Science* **1996**, *272*, 1924−1926. (f) Harfenist, S. A.; Wang, Z. L.; Alvarez, M. M.; Vezmar, I.; Whetten, R. L. *J. Phys. Chem.* **1996**, *100*, 13904−13910.

(4) (a) *Optical Properties of Metal Clusters*; Kreibig, U.; Vollmer, M., Eds. Springer-Verlag: New York, 1995. (b) Underwood, S.; Mulvaney, P. *Langmuir* **1994**, *10*, 3427−3430. (c) Mulvaney, P. *Langmuir* **1996**, *12*, 788−800. (d) Kreibig, U.; Fauth, K.; Quinten, M.; Schönauer, D. *Z. Phys. D* **1989**, *12*, 505.

(5) (a) Brust, M.; Walker, M.; Bethell, D.; Schiffrin, D. J.; Whyman, R. *J. Chem. Soc., Chem. Commun.* **1994**, 801−802. (b) Brust, M.; Fink, J.; Bethell, D.; Schiffrin, D. J.; Kiely, C. J. *J. Chem. Soc., Chem. Commun.* **1995**, 1655−1656. (c) Brust, M.; Bethell, D.; Schiffrin, D. J.; Kiely, C. J. *Adv. Mater.* **1995**, *7*, 795−797. (d) Bethell, D.; Brust, M.; Schiffrin, D. J.; Kiely, C. J. *J. Electroanal. Chem.* **1996**, *409*, 137−143.

S0743-7463(97)00588-X CCC: $15.00
Published on Web 01/06/1998

prepared in large quantities. Manipulation[5a,7a] of the preparative reaction conditions can effect changes in cluster dimensions; these monolayer-protected clusters (MPCs) are thus appealing for the study of size-dependent physical and chemical properties.

In this paper, we present the synthesis and characterization of a series of unfractionated (i.e., as-prepared) dodecanthiolate-protected Au cluster preparations. Average core diameters range from 1.5 to 5.2 nm; remarkably, even the smallest core sizes exhibit surface plasmon and electron binding energy properties that can be considered metallic, implying that the transition between molecular and metallic behavior lies at smaller core sizes.[8]

This paper also describes how the alkanethiolate monolayer changes as a function of Au core size. Alkanethiolate-protected Au clusters can be regarded as 3-dimensional (3D) analogs of self-assembled monolayers (3D-SAMs) formed by alkanethiolate ligands on flat Au surfaces (2D-SAMs).[9] Two structural features inherent in the Au cluster molecules, large populations of core surface Au atoms that on a flat surface would be regarded as defect sites, and a high radius of core curvature, promote differences between 3D- and 2D-SAMs. Fourier transform infrared (FTIR) spectroscopy has already detected examples of these dimensional distinctions; the conformational order of dropcast films of cluster compounds,[6c,7c] although strong, is less than that of a 2D-SAM of corresponding chainlength. These studies suggest that the structure (and perhaps reactivity) of the solid-state 3D-SAM should also depend on the size of the Au core, which is confirmed in the present case by FTIR spectroscopy, differential scanning calorimetry (DSC), mass spectrometry (MS), X-ray photoelectron spectroscopy, and contact-angle observations. Surprisingly, the disorder/order transition roughly marking the borderline between a 3D- and a 2D-SAM lies at a relatively small core size.

Experimental Section

Chemicals. $HAuCl_4 \cdot xH_2O$ was either purchased (Aldrich, 99.99%) or synthesized.[10] All other reagents were acquired from standard sources and used as received.

Synthesis. The syntheses followed a standard procedure,[6c] within which three reaction conditions were systematically varied (Table 1): (1) the temperature of the $NaBH_4$ reduction step; (2) the mole ratio of dodecanethiol:$HAuCl_4 \cdot xH_2O$; and (3) the rate of addition of $NaBH_4$.

To a vigorously stirred solution of 1.5 g of tetraoctylammonium bromide (2.5 equiv) in 80 mL of toluene was added 0.31 g of $HAuCl_4 \cdot xH_2O$ (1 equiv) in 25 mL of deionized water. The yellow $HAuCl_4 \cdot xH_2O$ aqueous solution quickly cleared and the toluene phase became orange-brown as the $AuCl_4^-$ was transferred into it. The organic phase was isolated, the desired amount of dodecanethiol was added, and the resulting solution was stirred for 10 min at room temperature. (For dodecanethiol:$AuCl_4^- \geq 2$, the orange-brown solution became either very pale yellow or colorless within 5 min.) Adjusting the solution temperature as desired for the reduction step, the reaction solution was then vigorously stirred and $NaBH_4$ (0.38 g, 10 equiv) in 25 mL of deionized water was added[11] over periods of either 10 s, 2 min, or 15 min (referred to as fd, md, and sd for fast, medium, and slow delivery, respectively). The now very dark organic phase was further stirred at the reduction temperature for 30 min and at room temperature for at least another 3 h. The organic phase was collected, and the solvent was removed on a rotary evaporator (for the larger clusters, this step should not exceed 50 °C to prevent partial product decomposition). The black product was suspended in 30 mL of ethanol, briefly sonicated to ensure complete dissolution of byproducts, collected on a glass filtration frit, and washed with at least 80 mL of ethanol and 150 mL of acetone. Upon air drying (or drying at room temperature in vacuo), materials were found to be spectroscopically (NMR) clean. The reactions have been successfully scaled up fivefold. These reactions were also carried out in oxygen−saturated/aerated solutions, but no evidence of oxygen-containing thiol or cluster products was ever seen (by ^{1}H NMR or MS).

Cluster Synthesis at −78 °C. This low temperature preparation (coded −78°,2X,sd) was identical to the aforementioned procedure except that the $NaBH_4$ reductant was suspended in 20 mL of absolute ethanol and added to a rapidly stirred $AuCl_4^-$/dodecanethiol toluene solution held at −78 °C (dry ice, acetone). Following addition of the reductant, the solution was stirred for 1 h at −78 °C, warmed slowly to room temperature, stirred an additional 3 h, and then worked up.

Spectroscopy (see Supporting Information for further details). Infrared absorbance spectra of clusters (either as dropcast thin films on KBr plates or pressed into a KBr pellet) were acquired using a Bio-Rad 6000 spectrometer. The ^{1}H and ^{13}C NMR spectra of C_6D_6 solutions were collected at 200 MHz and 50 MHz, respectively, on a Bruker AC200 spectrometer, and UV/vis spectra of hexane solutions with a ATI UNICAM spectrometer. X-ray photoelectron spectra for the gold clusters (dropcast from hexane onto a molybdenum substrate) were

(6) (a) Terrill, R. H.; Postlethwaite, T. A.; Chen, C.-H.; Poon, C.-D.; Terzis, A.; Chen, A.; Hutchison, J. E.; Clark, M. R.; Wignall, G.; Londono, J. D.; Superfine, R.; Falvo, M.; Johnson, C. S., Jr.; Samulski, E. T.; Murray, R. W. *J. Am. Chem. Soc.* **1995**, *117*, 12537−12548. (b) Hostetler, M. J.; Green, S. J.; Stokes, J. J; Murray, R. W. *J. Am. Chem. Soc.* **1996**, *118*, 4212−4213. (c) Hostetler, M. J.; Stokes, J. J.; Murray, R. W. *Langmuir* **1996**, *12*, 3604−3612. (d) Green, S. J.; Stokes, J. J.; Hostetler, M. J.; Pietron, J. J.; Murray, R. W. *J. Phys. Chem. B* **1997**, *101*, 2663. (e) Hostetler, M. J.; Murray, R. W. *Curr. Opin. Colloid Interface Sci.* **1997**, *2*, 42−50. (f) Ingram, R. S.; Hostetler, M. J.; Murray, R. W. *J. Am. Chem. Soc.* **1997**, *119*, 9175. (g) Ingram, R. S.; Hostetler, M. J.; Murray, R. W.; Schaaff, T. G.; Khoury, J. T.; Whetten, R. L.; Bigioni, T. P.; Guthrie, D. K.; First, P. N. *J. Am. Chem. Soc.* **1997**, *119*, 9279. (h) Templeton, A. C.; Hostetler, M. J.; Kraft, C. T.; Murray, R. W., submitted for publication.

(7) (a) Leff, D. V.; Ohara, P. C.; Heath, J. R.; Gelbart, W. M. *J. Phys. Chem.* **1995**, *99*, 7036−7041. (b) Badia, A.; Gao, W.; Singh, S.; Demers, L.; Cuccia, L.; Reven, L. *Langmuir* **1996**, *12*, 1262−1269. (c) Badia, A.; Singh, S.; Demers, L.; Cuccia, L.; Brown, G. R.; Lennox, R. B. *Chem. Eur. J.* **1996**, *2*, 359−363. (d) Whetten, R. L.; Khoury, J. T.; Alvarez, M. M.; Murthy, S.; Vezmar, I.; Wang, Z. L.; Stephens, P. W.; Cleveland, C. L.; Luedtke, W. D.; Landman, U. *Adv. Mater.* **1996**, *8*, 428−433. (e) Ohara, P. C.; Leff, D. V.; Heath, J. R.; Gelbart, W. M. *Phys. Rev. Lett.* **1995**, *75*, 3466−3469. (f) Luedtke, W. D.; Landman, U. *J. Phys. Chem.* **1996**, *100*, 13323−13329. (g) Weisbecker, C. S.; Merritt, M. V.; Whitesides, G. M. *Langmuir* **1996**, *12*, 3763−3772. (h) Leff, D. V.; Brandt, L.; Heath, J. R. *Langmuir* **1996**, *12*, 4723−4730. (i) Alvarez, M. M.; Khoury, J. T.; Schaaff, T. G.; Shafigullin, M. N.; Vezmar, I.; Whetten, R. L. *J. Phys. Chem. B* **1997**, *101*, 3706. (j) Cleveland, C. L.; Landman, U.; Shafigullin, M.; Stephens, P. W.; Whetten, R. L. *Z. Phys.D* **1997**, *40*, 503. (k) Vezmar, I.; Alvarez, M. M.; Khoury, J. T.; Salisbury, B. E.; Whetten, R. L. *Z. Phys. D* **1997**, *40*, 147. (l) Johnson, S. R.; Evans, S. D.; Mahon, S. W.; Ulman, A. *Langmuir* **1997**, *13*, 51−57. (m) Badia, A.; Cuccia, L.; Demers, L.; Morin, F.; Lennox, R. B. *J. Am. Chem. Soc.* **1997**, *119*, 2682−2692. (n) Yonezawa, T.; Tominaga, T.; Richard, D. *J. Chem. Soc., Dalton Trans.* **1996**, 783−789. (o) Alvarez, M. M.; Khoury, J. T.; Schaaf, T. G.; Shafigullen, M.; Vezmar, I.; Whetten, R. L. *Chem. Phys. Lett.* **1997**, *266*, 91. (p) Yonezawa, T.; Sutoh, M.; Kunitake, T. *Chem. Lett.* **1997**, 619. (q) Buining, P. A.; Humbel, B. M.; Philipse, A. P.; Verkleij, A. J. *Langmuir* **1997**, *13*, 3921. (r) Whetten, R. L., personal communication. (s) Andrews, R. P.; Bielefeld, J. D.; Henderson, J. I.; Janes, D. B.; Kolagunta, V. R.; Kubiak, C. P.; Mahoney, W. J.; Osifchin, R. G. *Science* **1996**, *273*, 1690−1693. (t) Andrews, R. P.; Bein, T.; Dorogi, M.; Feng, S.; Henderson, J. I.; Kubiak, C. P.; Mahoney, W.; Osifchin, R. G.; Reifenberger, R. *Science* **1996**, *272*, 1323−1325.

(8) Recent work in this lab indicates that the transition between metallic and molecular behavior occurs at a gold core size of ∼40 atoms; see ref 6g.

(9) (a) Dubois, L. H.; Nuzzo, R. G. *Annu. Rev. Phys. Chem.* **1992**, *43*, 437−463. (b) Ulman, A. *An Introduction to Ultrathin Organic Films*, Academic: New York, 1991. (c) Bain, C. D.; Whitesides, G. M. *Angew. Chem., Int. Ed. Engl.* **1989**, *28*, 506−512. (d) Ulman, A. *Chem. Rev.* **1996**, *96*, 1533−1554.

(10) (a) *Handbook of Preparative Inorganic Chemistry*; Brauer, G., Ed.; Academic: New York, 1965, pp 1054−1059. (b) Block, B. P. *Inorg. Syn.* **1953**, *4*, 14−17.

(11) The quantity of $NaBH_4$ reductant was also varied in the 0,2x,fd cluster preparation. Judging by ^{1}H NMR linewidths, increased amounts of $NaBH_4$ had no apparent effect; decreased amounts ($NaBH_4$:$AuCl_4^-$ mole ratios of 5:1 and 2:1) slightly increased average particle size (FWHM, 19 and 21 Hz, respectively). A mole ratio of 1:1 significantly increased particle size (FWHM = 32 Hz) with ∼50% toluene-insoluble product; a mole ratio of 1:2 gave only insoluble product.

collected on a Physical Electronics Industries 5500 surface analysis system with Al Kα source, hemispherical analyzer, torroidal monochromater, and multichannel detector (the pass energy was 187.9 eV, with a resolution of ~0.3 eV). The peak positions of *S* $2p_{3/2}$ and *S* $2p_{1/2}$ were determined by spectral deconvolution with a Gaussian-profile curve fitting with the constraint of a doublet of peaks with a FWHM of 0.90 ± 0.05 eV.[12] Peak positions were internally referenced to the *C* 1*s* peak (from the methylene chain of the ligand) at 284.9 eV.

Thermal Analysis (see *Supporting Information* for further details). The DSC was performed with a Seiko SSC 5200 thermal analysis system and thermogravimetric analysis (TGA) with a Seiko RTG 220 robotic TGA.

Contact Angles (see *Supporting Information* for further details). Advancing contact angles of interfaces of sessile water droplets and cluster films on smooth Au films were measured with a contact angle goniometer (Ramé-Hart, Inc.); data reported are averages from six different droplets.

Small-Angle X-ray Scattering (SAXS). Experiments on hexane cluster solutions in an airtight stainless steel cell with Mylar windows were performed on the Oak Ridge National Laboratory 10 m SAXS instrument[13ab] with sample−detector distances of 1.119 and 5.119 m using Cu Kα radiation ($\lambda = 1.54$ Å) and a 20 × 20 cm^2 area detector with cell size ~3 mm. The data were worked up as described previously.[6a,13c−h]

High-Resolution Transmission Electron Microscopy (TEM). Samples for TEM were prepared by dropcasting one drop of a ~1 mg/mL cluster solution in toluene onto standard carbon-coated (200−300 Å) Formvar films on copper grids (600 mesh) and drying in air for at least 45 min. Phase-contrast images of the particles were obtained with a side-entry Phillips CM12 electron microscope operating at 120 keV. Three typical regions of each sample were obtained at 580 000X. Size distributions of the Au cores were measured from enlarged TEM image photographs for at least 80−150 individual cluster core images.

Mass Spectrometry (see Supporting Information for further details). Thermal desorption experiments were performed with the direct insertion probe of a forward (EB) geometry Finnigan MAT 900 instrument using 70 eV electron ionization. The probe temperature was ramped to 200 °C in 1 min and then from 200 to 300 °C in 20 min at a rate of 5 °C/min, while scanning the spectrometer over a mass range of 40 to 481 Da at a rate of 1.1 scan/degree.

Results and Discussion

Synthesis. Small Au clusters protected by PR_3 ligands, such as those first reported by Schmid's group, have been known for some time.[1e,g] However, the reliable formation of larger and more stable MPCs remained for Brust et al.,[5a] who demonstrated that an organic-phase reduction of $HAuCl_4$ by dodecanethiol and $NaBH_4$ leads to stable, modestly polydisperse, dodecanethiolate-protected Au clusters with a central population of core dimensions 2.0−2.5 nm. Subsequent reports have shown that this basic protocol can give access to clusters protected by a range of alkanethiolate chain lengths (C3−C24)[6c] and functional groups,[5b,7b] and that variation[7a] of the RSH:$AuCl_4^-$ ratio (2:1 to 1:6) changes the cluster core size produced.

We have here extended the RSH:$AuCl_4^-$ mole ratio used in the Brust et al.[5a] reaction from 4:1 to 1:12, and have varied the temperature and rate of reductant addition as shown in Table 1 (see footnote *a* for coding of reaction conditions). The color and physical consistency of the product clusters vary substantially from the top to the bottom of the table, which is arranged (*vide infra*) from smallest to largest core sizes. For the smallest cores, the cluster material is black and waxy. With increasing core size (such as RT,1/2X,fd), the texture of the cluster material becomes "clumpy" and less waxy and then powdery but still black (such as RT,1/6X,fd). For the largest sizes (such as RT,1/10X,fd), the dark, free-flowing powder displays a distinct golden hue.

Table 1. Size and Composition Results for Different Cluster Preparations

preparation conditions[a]	SAXS[b] R_G, nm, max/min	SAXS[c] R_{POROD}, nm	HRTEM[d] R_{TEM}, nm	TGA[e] % organic	NMR[f] CH_3, ν_{FWHM} Hz
−78°,2X,sd	1.7/0.91	0.76	—	30.7	16
0°,2X,fd	—	—	1.1	28.8	21
0°,2X,md	—	—	—	26.7	22.5
0°,2X,sd	1.7/1.0	0.89	1.1	26.2	25.5
RT,1X,fd	1.7/1.2	1.0	—	25.6	24.5
RT,4X,fd	1.7/1.1	0.94	—	24.9	26
RT,2X,sd	1.6/1.2	0.96	—	24.5	27
RT,2X,fd	—	—	—	23.7	25.5
60°,2X,sd	1.4/1.2	0.98	—	24.1	29
90°,2X,sd	—	—	1.1	23.2	32
RT,1/2X,fd	1.6/1.4	1.2	1.2	19.4	37
RT,1/3X,fd	1.8/1.6	1.4	1.4	16.9	45
RT,1/4X,fd	2.1/2.0	1.7	2.0	12.8	53
RT,1/6X,fd	2.9/2.5	2.2	2.2	9.3	126[g]
RT,1/8X,fd	—	—	—	10.4	124[g]
RT,1/10X,fd	—	—	2.4	6.2	144[g]
RT,1/12X,fd	—	—	2.6	11.9	163[g]

[a] Code for preparation conditions: (*a*,*b*,*c*), where *a* represents the temperature at which the reduction was carried out, *b* represents the RSH:$AuCl_4^-$ molar ratio before reduction, and *c* represents the rate of reductant addition (fd, 10 s; md, 2 m; sd, 15 m). [b] SAXS results for Au core radius determined from Guinier plot. [c] SAXS results from Porod plot. [d] HRTEM results, average Au core size from analysis of histogram of HRTEM images. [e] TGA for thermal loss of alkanethiolate fraction of clusters. [f] Proton NMR linewidths. [g] CH_3 ^1H NMR signal obscured; the CH_2 resonance was used instead for these clusters.

In reactions with RSH:$AuCl_4^-$ mole ratios of ≥2:1, the orange-brown $R_4N^+AuCl_4^-$/toluene solution fades within 5 min after adding the alkanethiol, which may signify an alkanethiol-induced reduction to Au(I). Consistent with this hypothesis are (i) the formation of oxidized thiol (the corresponding disulfide, seen by NMR) as a major byproduct of the reaction, and (ii) the stoichiometric requirement of a threefold excess of thiol to completely reduce the metal center to Au(I).[7o] Also, literature syntheses for Au(I) alkanethiolate complexes, which are thought to be [Au-S(R)-]$_n$ polymers, follow a similar procedure.[14] In principle, forming a Au(0) cluster should require only a single further equivalent of reductant, but the Brust et al., procedure[5a] recommends a 10:1 BH_4^-:$AuCl_4^-$ ratio, as used in Table 1. Experiments[11] using less reductant yield clusters with increased average core size and larger quantities of insoluble matter, presumably aggregated cluster. The action of alternative reductants was not explored; the literature teaches[15] that in general, weaker reductants produce larger particles.

Cluster Size Determinations. Measurements on the cluster preparations, detailed in Table 1, were conducted with a combination of analytical tools: high-resolution

(12) Shirley, D. A. *Phys. Rev. B* **1972**, *5*, 4709−4714.

(13) (a) Hendricks, R. W. *J. Appl. Phys.* **1978**, *11*, 15. (b) Wignall, G. D.; Lin, J. S.; Spooner, S. *J. Appl. Crystallogr.* **1990**, *23*, 241−245. (c) Russell, T. P.; Lin, J. S.; Spooner, S.; Wignall, G. D. *J. Appl. Crystallogr.* **1988**, *21*, 629−638. (d) Guinier, A.; Fournet, G. *Small Angle Scattering of X-rays*; John Wiley: New York, 1955. (e) Glatter, O.; Kratky, O., Eds. *Small Angle X-ray Scattering*; Academic: New York, 1982. (f) Brill, O. L.; Weil, C. G.; Schmidt, P. W. *J. Coll. Interface Sci.* **1968**, *27*, 479−492. (g) Brill, O. L.; Schmidt, P. W. *J. Appl. Phy.* **1968**, *39*, 2274. (h) Motte, L.; Billoudet, F.; Pileni, M. P. *J. Phys. Chem.* **1995**, *99*, 16425−16429.

(14) (a) McNeillie, A.; Brown, D. H.; Smith, W. E.; Gibson, M.; Watson, L *J. Chem. Soc., Dalton Trans.* 1980, 767−770. (b) Puddephatt, R. J. In *Comprehensive Coordination Chemistry*, Wilkinson, G.; Gillard, R. D.; McCleverty, J. A., Eds.; Pergamon: New York, 1987; Vol. 5; pp 861−923.

(15) Hayat, M. A., Ed. *Colloidal Gold*; Academic: New York, 1989; Vol. 1.

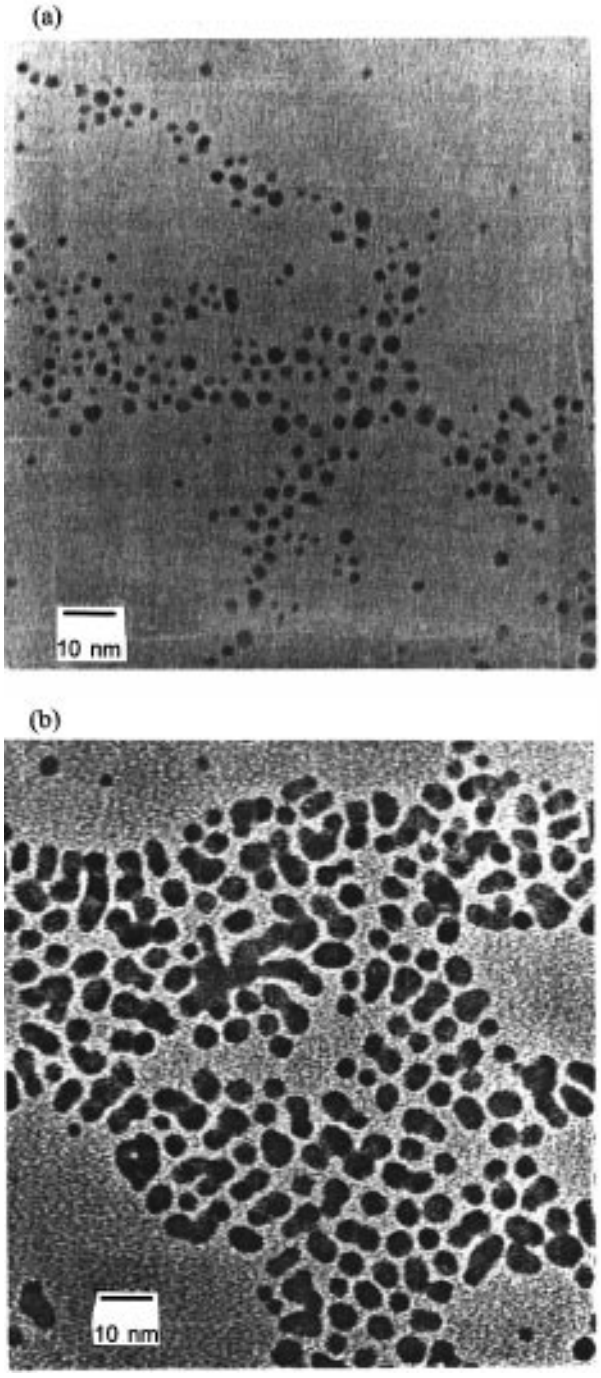

Figure 1. Transmission electron micrographs of dropcast films of dodecanethiolate-protected Au clusters: (a) (0°,2X,fd), (b) (RT, 1/6X,fd).

transmission electron microscopy (HRTEM) and small angle X-ray scattering (SAXS) for the Au core size, NMR spectroscopy for cluster size, and thermogravimetric analysis (TGA) for alkanethiolate ligand coverage. The results from these various techniques are remarkably consistent.

High-Resolution Transmission Electron Microscopy. HRTEM has been a potent tool in earlier investigations of the size and shapes of Au alkanethiolate cluster compounds.[5,7c−e] For example, HRTEM in the Brust et al.[5a] report led to an early estimate that the typical shape was either icosohedral or cuboctahedral; the latter shape (309 atom cuboctahedron) was assumed in our own early analysis.[6a] Later, TEM analysis of a fractionally crystallized sample, combined with matrix-assisted laser desorption ionization (MALDI) MS and theoretical calculations, determined that a more likely shape of the Au core is a truncated octahedron, and that preferred core Au atom populations ("magic numbers" or completed metal shells) include 225, 314, and 459 atom clusters.[7d] Interesting ordering features have also been uncovered by TEM; in 2D crystallites of polydisperse MPC samples, patterns of smaller clusters can form[7e] around larger ones, whereas in monodisperse samples, both long-range positional (*ca.* microns) and orientational ordering can be present.[7d] The cluster core−core distance visualized by TEM is often about the length of only one ligand chain.[7c−e]

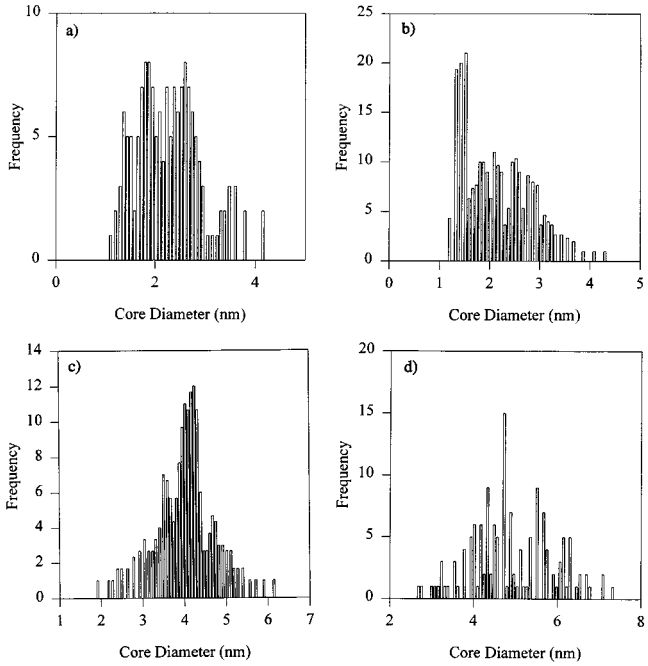

Figure 2. Size histograms (a and d are for films shown in Figure 1): (a) (0°,2X,fd); (b) (0°,2X,sd); (c) (RT,1/4X,fd); (d) (RT, 1/6X,fd).

In the present study, HRTEM images collected for a broad range of preparation conditions and thus core sizes are illustrated by representative examples (0°,2X,sd) and (RT,1/6X,fd) in Figure 1a and b, which display several notable, qualitative features. First, the clearly present dispersity in core size seems to be more prevalent for clusters prepared at lowered temperatures and (not shown) with slow addition of reductant. Second, packing order is higher for the larger clusters, which is consistent with previous studies.[7d] Third, the closest core−core spacing is uniform for each preparation and is approximately equal to the length of a single extended dodecanethiolate chain, supporting previous evidence[6a,7c−e] for the intercalation or interdigitation of alkyl chains or chain bundles of adjacent cluster molecules. The distance between two clusters is, however, often much larger than one chain length, reflecting significant packing disorder in the 2D structure. Fourth, although the images are not very distinct, the shapes are clearly not spherical. Finally, larger particles experienced some beam damage over time as evidenced by changes in core shapes, but the shape and size of smaller core cluster preparations appeared to be stable.

HRTEM core size histograms (Figure 2a−d) of selected preparations yield average core radii (Table 1, HRTEM column) in which RSH:$AuCl_4^-$ mole ratios of >1:1 lead to the smallest sizes and ratios of <1:1 yield lead to increasingly larger sizes. Many core size histograms (Figure 2a,c, and d) display multimodal distributions, the

maxima of which are generally repeated in other histograms (including examples not shown). These results indicate, in accord with previous work,[7d] a preference for certain cluster "magic numbers". Our data resolution is not fine enough, however, to verify if *only* magic number clusters are formed. The histograms also show that the main difference between clusters prepared by fast versus slow addition of reductant [compare (0°,2X,fd) versus (0°,2X,sd)] is not average core size, but rather its dispersity. The former material contains essentially equal populations of clusters with diameters of ~1.8 and ~2.6 nm with minor populations at ~1.4 and ~3.5 nm, whereas the latter material is composed of ~25% material with ~1.4 nm diameter, with the rest in a broad distribution centered at ~2.3 nm. These data suggest that in slow delivery of reductant, very small particles are formed initially (characteristic of a large RSH:$AuCl_4^-$ mole ratio), whereas later during delivery, depletion of thiol concentration leads to a progression of larger cores. Rapidly added reductant, on the other hand, quickly nucleates cores that grow within a more constant RSH:$AuCl_4^-$ mole ratio, yielding a more uniform core size.

Whetten et al.[7d] have shown that Au clusters prepared by the Brust et al.[5a] method can be fractionated into monodisperse samples, and the materials described here can also be fractionated by successive precipitations. Fractionated samples tend to yield small quantities of materials, whereas synthetic elaboration of clusters is aided by generous and readily available supplies. Because the chemistry of functionalized cluster molecules is a vitally important part of this emerging field, and we have undertaken synthetic investigations[6f,h] that involve availability of clusters characterized in terms of average core dimensions, we did not attempt to fractionate the preparations used in this report. Judicious choice of the preparation conditions, in combination with fractionation, should lead to future procedures for production of large quantities of monodisperse nanoparticles over a large range of sizes.

Small-Angle X-ray Scattering (SAXS). Metal clusters with hydrocarbon ligands and in hydrocarbon solvents are ideal SAXS substrates because the X-ray scattering is dominated by the metal core and contributions from the ligand shell and solvent are minimal. SAXS data, collected for about one-half of the cluster preparations, exhibited large signal-to-noise ratios and intensities (I) scaling linearly with concentration (i.e., cluster−cluster scattering is unimportant).

The cluster core sizes were deduced from the SAXS data based on two approaches (Table 1). Guinier plots (log I *versus* Q^2 is linear) taken over small and large scattering angles serve to estimate the largest and smallest core sizes (R_G), respectively, present in sufficient quantities to appreciably contribute to the scattered intensity. At small scattering angles [$Q = 4\pi(\sin\theta)/\lambda$, where λ is wavelength and 2θ the angle of scatter, thus Q is typically in units of $Å^{-1}$], the largest clusters dominate the scattering, whereas at higher scattering angles, the smaller particles dominate. Thus, the R_G radius of larger particles was calculated from Q^2 between ~0.002 and 0.0112, whereas evaluation of the smaller particle sizes relied on Q^2 between ~0.03 and 0.115. These data are given in Table 1 as R_G(max/min). The second SAXS data analysis used Porod plots ($Q^4I(Q)$ *versus* Q, see examples in Figure 3), the maxima of which can give reliable estimates ($0.54/Q_{MAX}$ = diameter in nm)[13h] of core size because the Au/ligand interface has a sharp transition in electron density. For some of the data, the scattered intensity was also fit assuming either monodisperse ellipsoidal (R_{MAX}/R_{MIN} = 1.4) or polydisperse spherical particles. These analyses demonstrated that the Porod plots reasonably estimate the radius of the smallest particles that have a significant population in the size dispersion. These values are given in Table 1 as R_{POROD}.

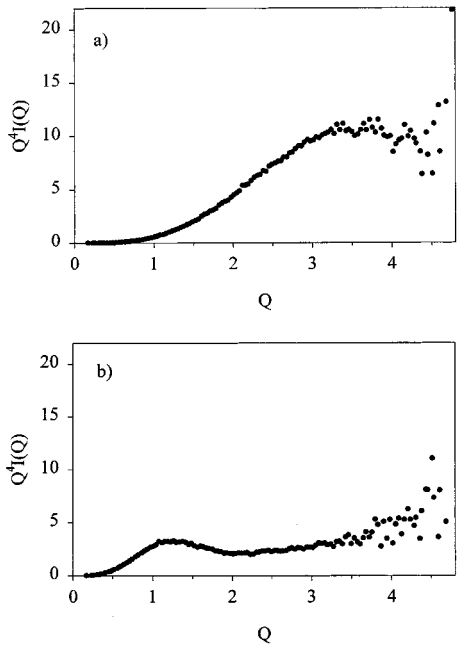

Figure 3. Porod plots of small-angle X-ray scattering data for dodecanethiolate-protected Au clusters: (a) (−78°,2X,sd); (b) (RT,1/6X,fd). Q in $Å^{-1}$.

We regard the best SAXS estimates for the largest and the smallest cluster core sizes as the Guinier results (R_G(max)) and the Porod results (R_{POROD}), respectively. Both R_{POROD} and R_G(min) nicely compare to R_{TEM}. In contrast, the SAXS maximal radii R_G(max) are considerably larger, reflecting the fact that the HRTEM values are averages from histograms; that is, numerically, the larger radii clusters constitute a minority population in the preparations. The SAXS results also agree with the HRTEM results in showing (a) that the smallest cluster cores are made at lower reaction temperatures and a high RSH:$AuCl_4^-$ mole ratio, whereas larger ones are products of low RSH:$AuCl_4^-$ mole ratios, and (b) [by the differences in R_G(min) and R_G(max)] that polydispersity (in terms of percent standard deviation) is more prevalent at lower reaction temperatures and high RSH:$AuCl_4^-$ mole ratios and less prevalent when low RSH:$AuCl_4^-$ mole ratios are used. Implications of and exceptions to these generalizations will be discussed later.

Thermogravimetric Analysis and Monolayer Coverage. The TGA results are also presented in Table 1. We have shown[6a] previously that TGA yields an organic weight fraction for the clusters that is consistent with their elemental analysis. Mass spectral results (*vide infra*) show that the material thermally desorbed is predominantly the corresponding disulfide and does not contain Au; visual inspection shows that the material remaining after thermolysis is essentially pure Au. Experiments are in progress to analyze and understand the structure of this Au residue.

Qualitatively, one expects that the weight fraction of alkanethiolate in the clusters should parallel the cluster core size, and this expectation is realized in the experimental results of Table 1. Data for a series of models in which core size and the corresponding TGA percent organic are calculated for different choices of core shape, assuming

Table 2. Results from Modeling of Gold Core Sizes, Shapes, and Alkanethiolate Coverages, and of Size-Dependent T_2 Broadening of Proton NMR of CH_3 Resonances

#atoms (shape)[a]	R_{CORE}, nm	#surface atoms/ %defect/area nm^2	calc TGA %organic/ %coverage/#chains	calc R_{TOTAL}, nm	calc NMR ν_{FWHM}, Hz
79 (TO^+)	0.65	60/60%/8.30	33.0/63%/38	2.6	15
116 (TO^-)	0.71	78/61%/11.36	31.8/68%/53	2.6	16
140 (TO^+)	0.81	96/50%/11.43	27.9/55%/53	2.7	17
201 (TO)	0.87	128/47%/15.22	26.5/55%/71	2.8	18
225 (TO^+)	0.98	140/43%/15.19	24.4/51%/71	2.9	19
309 (CO)	1.1	162/52%/19.64	23.3/57%/92	3.0	22
314 (TO^+)	1.0	174/41%/19.46	22.9/52%/91	3.0	20
459 (TO^+)	1.2	234/36%/24.34	20.2/49%/114	3.1	23
586 (TO)	1.2	272/35%/28.94	19.1/50%/135	3.2	24
807 (TO^+)	1.4	348/31%/34.86	17.1/47%/163	3.3	27
976 (TO^-)	1.5	390/31%/40.02	16.4/48%/187	3.4	28
1289 (TO)	1.6	482/27%/47.22	14.9/46%/221	3.5	32
2406 (TO)	2.0	752/22%/69.86	12.2/43%/326	3.9	42
2951 (TO^+)	2.2	876/21%/79.44	11.4/42%/371	4.1	47; 94[b]
4033 (TO)	2.4	1082/19%/97.00	10.3/42%/453	4.3	55; 110[b]
4794 (TO^+)	2.6	1230/18%/108.28	9.7/41%/506	4.4	61; 122[b]
6266 (TO)	2.8	1472/16%/128.66	8.9/41%/601	4.7	70; 140[b]

[a] CO = cuboctahedron; TO = ideal truncoctahedron (all sides equal); TO^+ = truncoctahedron in which ($0 < n - m \leq 4$), where n is the number of atoms between (111) facets and m is the number of atoms between (111) and (100) facets; TO^- = truncoctahedron in which ($-4 \leq n - m < 0$, $m > 1$). [b] The second value is the calculated linewidth for the methylene peak.

maximal alkanethiolate coverage, are shown in Table 2. For the core shape, we use truncated octahedra as advocated by Whetten et al.,[7d] except for the ~300 atom core where a (309 atom) cuboctahedral example[16] is given to emphasize the general similarity of the numbers to a 314 atom truncated octahedron.[16] On a very large cluster, the calculated %coverage (100 × thiolate per surface Au atom) approaches that of a flat Au(111) surface (i.e., 33%).[9a] A previous analysis[6a] of results based on a Au-309 cuboctahedral cluster gave a 66% coverage, reflecting the combination of a large proportion of edge and corner atoms on these nanoparticles[17] and their high radius of curvature. The questions become then, how closely does experimental %coverage on even larger core size clusters actually approach the 33% 2D-SAM result and, conversely, for the smallest core size clusters, how closely is the 100% "coverage" (e.g., 1:1 mole ratio) of a [AuSR] compound approached?

The relationship between core size and TGA %organic was analyzed by two methods.[18] In Method 1, the surface areas of ideal polyhedra[19] (Table 2) were divided by the surface area footprint of an alkanethiolate ligand (0.214 nm^2),[20] which gives for each polyhedron size the number of alkanethiolate chains, a calculated "TGA %organic", and (using the number of surface Au atoms) a calculated %coverage. These values are listed in Table 2 with the average radii of the various polyhedra. The calculated TGA %organic and %coverage values are maximal for each polyhedron because the calculation presumes a sterically limiting fit of ligands on each surface. The calculations in Table 2 can be compared with the experimental data in Table 1 by selecting the model polyhedral core size and calculated TGA %organic that together best match the experimental values. Thus, for example, the experimental TGA %organic for the (−78°,2X,sd) cluster preparation is 30.7%; from Table 2 an estimated maximum average core size for this preparation is the 116 atom cluster because the calculated maximum coverage for that cluster size is 31.8%.

In Method 2, average core sizes of model polyhedra (in Table 2) that best match the Table 1 SAXS and HRTEM results are used along with the experimental TGA results to calculate an experimental %coverage for the various preparations (given in Table 3). In general, the calculated Table 2 and experimental Table 3 %coverages are quite close, indicating that a reasonable assignment is made in Table 3 for the core size that is most prevalent for each synthetic preparation. In some cases, the comparisons suggest a mixture of two dominant polyhedral sizes, such as for the (0°,2X,fd) preparation that appears to be a mixture of the 116 and 140 atom cores. In the case of the (90°,2X,sd) cluster preparation, the experimental coverage (Table 3) is significantly smaller than that calculated in Table 2, a discrepancy that can be rationalized by some cluster decomposition at the elevated reaction temperature.

Overall, the combined analysis of SAXS, HRTEM, and TGA results produces in Table 3 a preparation-dependent scale of average cluster polyhedral sizes that is remarkably self-consistent.

NMR Spectroscopy. The ^{1}H and ^{13}C NMR spectra of solutions of the Au clusters are characteristically broadened relative to those of free alkanethiols. The ^{13}C NMR spectra of alkanethiolate-protected Au clusters reveal[6a,7b] that linewidths vary systematically with carbon site position relative to the Au core surface. Thus, the octanethiolate ligand methyl ^{13}C (and ^{1}H) resonances are broader than those of a dodecanethiolate ligand, and ^{13}C methylene linewidths increase throughout with proximity to the thiolate/Au interface.

(16) Our previous analysis[6a] assumed cuboctahedra as advocated originally by Brust et al.[5a]

(17) A sphere, covered by tightly packed alkanethiolate ligands can achieve a maximum coverage of 43%; thus, the presence of faces, edges, and corners significantly increases the ligand density of a polyhedron with the same average diameter.

(18) Polydispersity of cluster sizes in a preparation will bias the calculated surface coverage; thus, these results only apply to a hypothetical average cluster size.

(19) The surface area calculation involved the assumptions: (a) flat polyhedra faces with dimensions determined by a Au atom diameter (0.288 nm) multiplied by the number of Au atoms on each edge; (b) area contributed from atoms on edges is counted twice and that from corner atoms three times. For example, for the Au-309 cuboctahedron there are six 5 × 5 square faces and eight equilateral triangular faces having edges of five Au atoms. The calculated surface area would then be $6[(5\cdot0.288)^2]$ (from the square faces) + $8[(5\cdot0.288)(2.5\cdot0.288)]$ (from the triangular faces), or 20.74 nm^2. Simple geometric considerations reveal that this calculation is equivalent to using 57% of the surface area of each edge Au atom and 83% of each corner Au atom. These contributions will clearly overestimate the actual surface area of the polyhedron; thus, coverages obtained from these calculations should be considered maximum values. Also latent in these assumptions is the approximation that the alkanethiolates will indiscriminately bind to the polyhedron to form a maximally packed surface.

(20) Sellers, H.; Ulman, A.; Schnidman, Y.; Eilers, J. E. *J. Am. Chem. Soc.* **1993**, *111*, 9389−9401.

Table 3. Cluster Core Size Assignments: Reconciliation of Cluster Coverages Based on SAXS, TGA and HRTEM-Determined Core Radii and Presumed Polyhedral Shapes, and of NMR Line Broadening with Estimated Core Radii

preparation conditions	core radius R_{AVG}, nm	# atoms in avg cluster	TGA expt. %coverage, avg. cluster	ratio expt. ν_{FWHM} to calc. ν_{FWHM}
−78°,2X,sd	0.76	116	64	1.0
0°,2X,fd	0.96	116/140	59	1.31, 1.24
0°,2X,md	0.98	201	55	1.25
0°,2X,sd	0.98	201/225	55	1.42, 1.34
RT,1X,fd	1.0	225/314	57	1.29, 1.22
RT,4X,fd	1.0	225/314	55	1.37, 1.3
RT,2X,sd	1.0	225/314	54	1.42, 1.35
RT,2X,fd	1.0	225/314	52	1.34, 1.28
60°,2X,sd	1.0	225/314	53	1.53, 1.45
90°,2X,sd	0.96	201	46	1.78
RT,1/2X,fd	1.4	586	51	1.54
RT,1/3X,fd	1.5	976	50	1.61
RT,1/4X,fd	2.2	2406	46	1.26
RT,1/6X,fd	2.2	2951	34	1.34
RT,1/8X,fd	2.2	2951	38	1.32
RT,1/10X,fd	2.4	4033	24	1.31
RT,1/12X,fd	2.6	4794	51[a]	1.34

[a] Unusually high value is likely due to coadsorbed solvent or tetraoctylammonium cations.

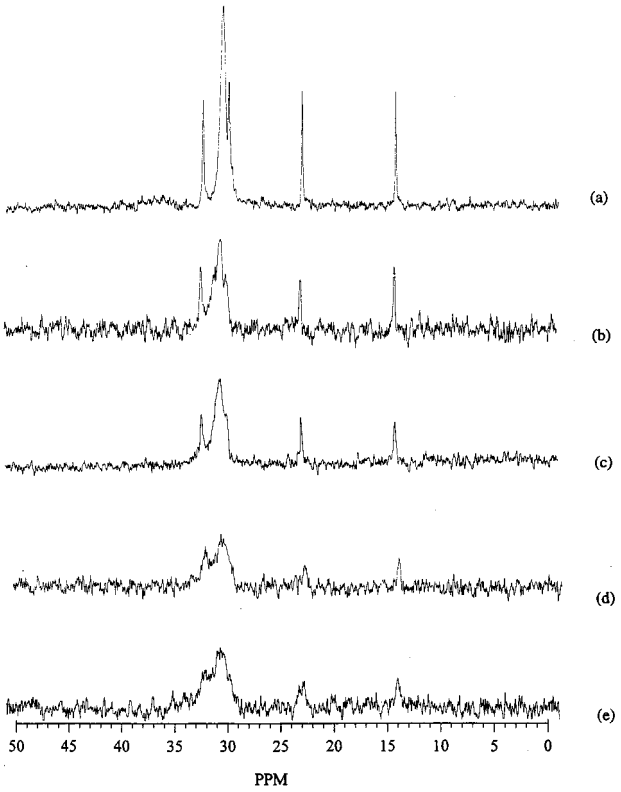

Figure 4. The ^{13}C NMR spectra (C_6D_6) of dodecanethiolate-protected Au clusters. Each spectrum was Fourier transformed using a line broadening of 3 Hz: (a) (−78°,2X,sd); (b) (90°,2X,sd); (c) (RT,1/3X,fd); (d) (RT,1/4X,fd); (e) (RT,1/6X,fd).

Multiple factors appear to contribute to the spectral broadening: (a) Methylenes closest to the thiolate/Au interface are the most densely packed and solid like, and thereby experience fast spin relaxation from dipolar interactions. Methylenes furthermost from the Au core experience freedom of motion and spin relaxations more similar to those of dissolved species.[6a,7b] This broadening effect thus rests on structural features of the monolayer. (b) The distribution of chemical shifts caused by differences in the Au−SR binding site (terraces, edges, vertices) was

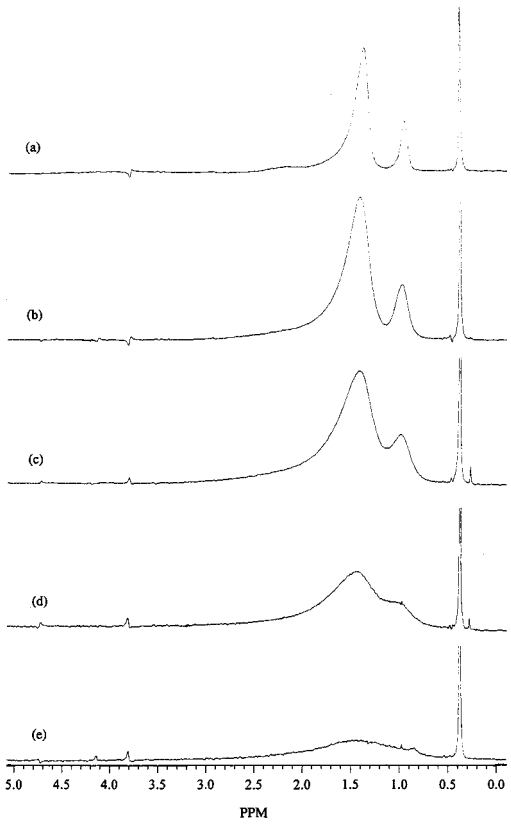

Figure 5. The ^1H NMR spectra (C_6D_6) of dodecanethiolate-protected Au clusters. Each spectrum was Fourier transformed using a line broadening of 1 Hz: (a) (−78°,2X,sd); (b) (90°,2X,sd); (c) (RT,1/3X,fd); (d) (RT,1/4X,fd); (e) (RT,1/12X,fd).

recently proposed to be responsible for the substantial broadening of the ^{13}C resonance for the α- and β-CH_2 groups in a solid-state Au cluster sample.[7b] This effect falls off sharply with distance from the metal core. (c) Spin−spin relaxation (T_2) broadening depends on the rate of tumbling of the cluster molecules in solution, and for the methyl resonance should vary as r^{-3}, where r is the average methyl-to-Au core center distance. We observe that the width of methyl group resonances varies systematically with core size and present here the first evidence for the quantitative importance of T_2 broadening for the Au cluster NMR resonances in solutions.

Figure 4 shows ^{13}C NMR spectra of cluster solutions (Au core size increases from top to bottom) that are consistent with all three broadening mechanisms: (a) The methyl (most upfield) resonance is consistently the sharpest of the spectrum. (b) For the smallest core size (Figure 4a), the β-methylene resonance is a broad, weak peak at ∼38 ppm, near that observed in the solid-state NMR studies.[7b] The smallest clusters have fewer different types of binding sites (dominantly vertices), thus diminishing effects due to chemical shift distributions. (c) A third noticable feature of Figure 4 is that the linewidths (ν_{FWHM}) increase with Au core size. Because the alkanethiolate chain length is constant, the change in ν_{FWHM} is more plausibly related to a core size-dependent variation in T_2 relaxation than to changes in dipolar broadening. We turn to the ^1H NMR spectra (Figure 5) for analysis of this relationship. Table 1 reports the proton resonance ν_{FWHM} data for the methyl group resonances (at 0.8 ppm, for exceptions, see footnote *g*, Table 1).

It is well known that NMR line broadening for proteins and polymers is dominated by their slow rotation in solution; the alkanethiolate-protected clusters are analo-

gous, slowly rotating macromolecules. Thus, ν_{FWHM} of the cluster methyl peak is related to the T_2* relaxation time (which is a combination of spin−spin relaxation and instrumental field inhomogeneity) by:

$$\nu_{FWHM} = 1/\pi T_2^* \quad (1)$$

The correlation time (τ_c) for spin−spin relaxation (that required for the molecule to rotate by 1 radian) can be calculated from the Stokes-Einstein equation:

$$\tau_c = (4\pi\eta r^3)/(3kT) \quad (2)$$

Equation 2 is qualitatively consistent with behavior of ^{1}H NMR spectra of the alkanethiolate Au clusters; line broadening progressively increases with increasing solvent viscosity (methylene chloride, chloroform, toluene, and benzene were examined) and increases at lowered probe temperature (down to −30 °C, where clusters precipitated from solution).

The full equation for the spin−spin relaxation time (and thus the linewidth) is[21a] :

$$1/T_2 = (3\mu_o^2\hbar^2\gamma^4)/(302\pi^2 b^6)[3\tau_c + 5\tau_c/(1 + \omega^2\tau_c^2) + 2\tau_c/(1 + 4\omega^2\tau_c^2)] \quad (3)$$

where μ_o is the vacuum permeability, γ the proton gyromagnetic ratio, ω the Larmor frequency (200 MHZ), and b the distance between spins.[21b] In comparing values for the various cluster preparations, all parameters in eq 3 except the methyl core radius r (which via eq 2 determines τ_c) are assumed to remain constant. Using these relations and the core size assignments made in Table 3 from comparisons of SAXS, HRTEM, and TGA observations, the ratio of experimental methyl ν_{FWHM} for pairs of cluster compounds can be used to calculate the ratio of their radii. Choosing one cluster as a reference point [that with the smallest ν_{FWHM}, the (−78°,2X,sd) preparation], ν_{FWHM} can be predicted for the other cluster preparations. These predictions are shown in Table 2 and are compared in Table 3 with the Table 1 experimental ν_{FWHM}. With only a few exceptions, the experimental linewidths track the calculated ones with a roughly constant, 30−40% offset.

Implicit in the aforementioned ν_{FWHM} analysis are several assumptions: (a) Any broadening of the methyl group resonance by dipolar interactions is core size independent. Thus, the ligand shell of dissolved clusters is regarded as having a densely packed, solid-like region near the Au surface and a free-draining region near the chain termini, with relatively mobile chain ends. This picture is consistent with the observation that hydrodynamic radii observed by diffusion-ordered spectroscopy (DOSY)[6a] for alkanethiolate-stabilized Au clusters are substantially smaller than R_{TOTAL}, the sum of the Au core radius and a fully extended alkyl chain length (Table 2). (b) The parameter r in eq 3 is taken as R_{TOTAL}; this approximation is admittedly imperfect based both on assumption a and FTIR evidence (*vide infra*) suggesting that chain conformation generally becomes more fully extended as the core size increases. Remembering, however, that ν_{FWHM} is a cubic function of r, minor adjustments of the assumed chain conformation would improve the fit between experimental and calculated ν_{FWHM}. (c) All clusters have many different types of ligand binding sites. Thus, line broadening, which may arise from this distribution, occurs approximately equally for all cluster sizes. (d) Each preparation gives monodisperse cluster sizes. Although this is clearly not the case, the preponderance of the proton peak intensities and associated ν_{FWHM} must arise from the particles of greatest concentration, which excludes the minority populations seen in HRTEM images. (e) The smallest, reference-size cluster is a 110 atom truncated octahedron.

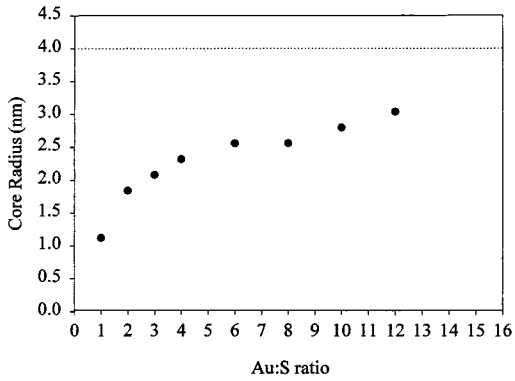

Figure 6. Plot of the cluster core radius, calculated from ^{1}H NMR line widths, as a function of Au:S ratio using during the cluster synthesis.

Given the general correspondence between the NMR and HRTEM, SAXS, and TGA results in Table 3, these assumptions and the analysis of the methyl resonance broadening as a cluster core size-dependent spin−spin relaxation effect seem reasonably justified.

Comments Regarding Synthetic Control of Core Size. The four methods used each rely on different information, but give the same ordering of reaction conditions as to obtained average core size, with the actual values being reasonably close. The easiest method to implement for routine studies is NMR line broadening, which slightly overestimates core size; however, TGA offers, for small core sizes, a greater sensitivity to size.

The results show that it is possible to select for cluster core size via the preparation conditions. For example, the core size decreases with increasing thiol:Au mole ratio (Tables 1−3); thiol excesses larger than the 2:1 used in the (−78°,2X,sd) preparation have been recently shown to produce average cluster core dimensions smaller than ∼1.6 nm.[7o] The (−78°,2X,sd) preparation clearly contains some clusters <1.6 nm as shown both by histograms of a HRTEM image and by a preliminary MALDI MS experiment (not shown) with mass/charge maxima at 15K Da (75 atoms) as well as at 23K (116 atoms) and 29K (147 atoms).[22] Also, the core size scale in Table 3 is specific for C12 alkanethiolate-protected clusters, and the scale may be shifted by using other ligand chainlengths.[7r]

Low thiol:Au mole ratios yield large core sizes, the limit of which is expected when the alkanethiol is omitted altogether. Brust et al.[5c] have reported this experiment, which gave a Au core with a 8.0 nm average diameter. Consistent with this result, our core diameters asymptotically change with Au:thiol ratios towards a value of ∼7 nm (Figure 6). Indeed, the core size becomes marginally sensitive to the Au:thiol ratio when the relative thiol concentration is very lean.

Our results differ, on the other hand, from those of Leff et al.[7a] who report, based on X-ray powder diffraction

(21) (a) Homans, S. W. *A Dictionary of Concepts in NMR*; Clarendon: Oxford, 1989. (b) *b* is the distance between like spins that can promote the relaxation of an excited spin (e.g., the distance between protons on the same CH_3 group).

(22) We thank Professor Robert L. Whetten, Igor Vezmar, and T. Gregory Schaaff of the School of Physics at the Georgia Institute of Technology for the acquisition of this data.

pattern line broadening, that core diameters from ~1.5 to as large as 16 nm can be synthesized by varying the C12 thiol:Au ratio in the Brust et al.[5a] reaction from 2:1 to 1:6 Both we and Brust observe the formation of much smaller core sizes than the Leff report under thiol-lean and -absent conditions, respectively. Our size measurements offer the confidence given by a battery of tools that agree with one another; the Leff et al.[7a] results may have been affected by sample aggregation during X-ray exposure. Our experience shows that the larger core sizes are especially sensitive to temperature and light and can decompose and aggregate to form larger particles under a beam of X-rays (however, aggregation was not observed while collecting the HRTEM images).

The effect of the reductant addition rate on the core size dispersity is an intriguing result. It seems that slow addition of reductant initially exposes the reduced Au to a very large excess of alkanethiol, thereby generating many small cores, as seen in the TEM image for the (0°,2X,sd) cluster synthesis. However, later during reductant addition, the available alkanethiol excess gradually diminishes and core sizes produced increase. In general, the extent of size dispersity decreases with increasing rate of reductant addition, an observation suggestive that an even larger excess of reductant, rapidly added, may further reduce both core size and dispersity.

Overall, the results show that the thiol:Au ratio has the greatest effect on cluster core size, the temperature at which reduction occurs affects the dispersity level with elevated temperature[23] also affecting completeness of the protecting monolayer, and the rate of reductant addition exercises the most control over the cluster dispersity.

Correlations of Core Electronic Properties with Core Size. As noted in the *Introduction*, although other studies have described relationships of metal cluster size to optical, electronic, magnetic, and catalytic properties, data for very small metal clusters are sparse.[4a,7d,i,8] This section presents UV/vis and X-ray photoelectron spectroscopic (XPS) observations for the alkanethiolate-protected Au clusters that reveal core-size-dependent electronic properties.

X-ray Photoelectron Spectroscopy. All previous XPS measurements[24a] on 2D-SAMs on Au (where alkanethiolate coverage is 33%) have produced Au $4f_{7/2}$ binding energies (84.0 ± 0.1 eV) similar to that of bulk Au (84.0 eV).[24b] On dodecanethiolate-protected Au nanoclusters (diameter, 2.0−2.5 nm; ~60% coverage based on a ~309 atom core), Brust et al.[5a] observed a Au $4f_{7/2}$ peak value of 83.8 eV, which tends toward the value seen for a surface layer of bare Au (83.6 eV).[25] It was thus of interest to see whether smaller cluster cores would continue to exhibit this bulk metal-like photoionization.

Table 4. X-ray Photoelectron Spectroscopy Data on Gold Clusters[a]

cluster	Au $4f_{7/2}$ (FWHM)[a]	*C* 1*s* FWHM[a,b]	*S* $2p_{1/2}$, *S* $2p_{3/2}$[a]	Au:S
−78°,2X,sd	84.4 (1.22)	1.22	163.4, 162.3	2.5
90°,2X,sd	84.2 (1.07)	1.17	163.5, 162.3	3.6
0°, 2X, fd	84.3 (1.12)	1.18	163.5, 162.3	2.7
0°, 2X, sd	84.1 (0.93)	1.25	163.2, 162.1	6.2
RT, 1/2X, fd	84.0 (0.98)	1.27	163.3, 162.1	6.5
RT, 1/10X, fd	84.0 (0.91)	1.29	163.2, 162.1	11.6

[a] In units of eV. [b] Samples were calibrated by assigning the *C* 1*s* peak a value of 284.9 eV.

In the present study, dropcast cluster films were examined and internally referenced to the *C* 1*s* peak (284.9 eV), which was assumed to be invariant with core size. Table 4 shows that Au $4f_{7/2}$ peak and the *S* 2*p* peaks are slightly sensitive to core size relative to the *C* 1*s* band, with both sets of peaks generally appearing at higher binding energies as the core size decreases. Thus, the Au $4f_{7/2}$ peak for the largest clusters appears at the same binding energy as a tested sample of bulk Au, whereas the same peak for the smaller clusters approaches the value previously observed for the Au(I) octanethiolate polymer (84.9 eV).[14a] In the case of the *S* 2*p* emission couplet, the band energies for the larger clusters are the same as those found for 2D-SAMs of dodecanethiol on Au(111). However, there is a subtle shift (0.2−0.3 eV) toward higher binding energies for the smaller-sized particles, which is in the direction of that seen for Au−SR compounds (0.7 eV higher than on a Au surface).[26] This shift is in the opposite direction from that observed for alkanethiolates bound to rough (high-step density) gold films.[24c]

The peaks for the smaller core sizes are shifted to higher binding energy, suggesting either a change in the nature of the Au−S bond (i.e., approaching that of a Au:alkanethiolate complex) or the increasing influence of final state charging effects.[25] It should be noted, though, that the observed shifts are relative to the *C* 1*s* peak of the alkanethiolate ligands, suggesting that if final-state charging effects are operative, their most significant influence is on the core rather than on the remainder of the sample. In either case, the small value of the shift indicates that any change in the nature of the Au core is subtle, at best. The loss of bulk properties and appearance of molecular characteristics in sufficiently small nanoscopic materials is popularly termed a "quantum size effect". Although well developed[3c] for semiconductor materials, examples showing the onset of this behavior for metal clusters are quite rare.[2,27]

Table 4 shows apparent Au:S atom ratios calculated from integrated Au $4f_{7/2}$ and the *S* 2*p* peak intensities measured in high-sensitivity scans. The three smallest and three largest clusters track Au:S ratios inferred from the TGA data to within 10 and 25%, respectively. This comparison ignores photoelectron escape depth considerations, and the agreement seen probably reflects the

(23) The cluster (90°,2X,sd) has an experimental NMR linewidth broader than predicted, and an experimental coverage smaller (i.e., its NMR line broadening and TGA %organic predict an average core size significantly larger than observed by HRTEM). It is difficult to reason how the HRTEM images could be so radically incorrect, so some aspect of this sample is different, such as a partial monolayer coverage of the cluster cores, with a resulting disorder that yields additional line broadening. That incomplete monolayer formation may arise from partial monolayer decomposition at elevated temperature is confirmed by heating of a toluene-d_8 solution of the (0°,2X,sd) cluster preparation at 90 °C, which leads (shown by NMR) to partial monolayer decomposition (<15%), forming di(dodecyl)disulfide and a cluster material that was still stable. Current studies demonstrate that alkyldisulfides cannot exchange onto clusters, so formation of dodecyldisulfide during (90°,2X,sd) cluster synthesis would not allow the full monolayer reconstitution even after the reaction was returned to room temperature.

(24) (a) Bain, C. D.; Biebuyck, H. A.; Whitesides, G. M. *Langmuir* **1989**, *5*, 723−727. (b) Hüfner, S. *Photoelectron Spectroscopy*, 2nd Ed.; Springer-Verlag: New York, 1996. (c) Porter, M. D., unpublished results.

(25) van der Putten, D.; Zanoni, R.; Coluzza, C.; Schmid, G. *J. Chem. Soc., Dalton Trans.* **1996**, 1721−1725.

(26) (a) A report of a 163.9 eV *S* 2*p* binding energy on 2D-SAMs[26b] has been refuted by a later report convincingly assigning this feature to physisorbed alkanethiols and/or dialkyldisulfides because thorough rinsing removed all trace of the 163.9 eV peak.[26c] In the present case, no free alkanethiol or dialkyldisulfide can be detected by ^{1}H NMR spectroscopy, so it is highly unlikely that such species could contribute any XPS band intensity. (b) Zubragel, Ch.; Deuper, C.; Scheider, F.; Neumann, M.; Grunze, M.; Schertel, A.; Woll, Ch. *Chem. Phys. Letters* **1995**, *238*, 308−312. (c) Castner, D. G.; Hinds, K.; Grainger, D. W. *Langmuir* **1996**, *12*, 5083−5086.

(27) Volokitin, Y.; Sinzig, J.; de Jongh, L. J.; Schmid, G.; Vargaftik, M. N.; Moiseev, I. I. *Nature* **1996**, *384*, 621−623.

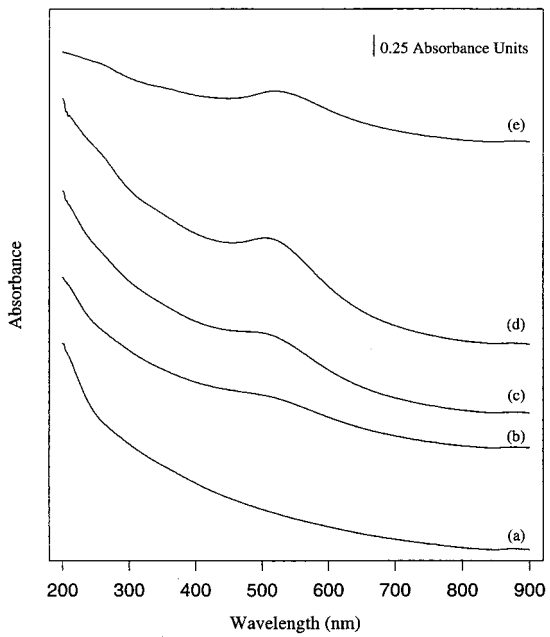

Figure 7. The UV/vis spectra (hexane) of dodecanethiolate-protected Au clusters: (a) (−78°,2X,sd), C = 3 × 10^{-6} M, MW = 3.4 × 10^4 amu; (b) (90°,2X,sd), C = 2 × 10^{-6} M, MW = 5.5 × 10^4 amu; (c) (RT,1/3X,fd), C = 4 × 10^{-7} M, MW = 2.3 × 10^5 amu; (d) (RT,1/4X,fd), C = 2 × 10^{-7} M, MW = 5.5 × 10^5 amu; (e) (RT,1/12X,fd), C = 9 × 10^{-8} M, MW = 1.1 × 10^6 amu.

large relative proportion of surface atoms in the Au atoms of a cluster core.

UV/vis Spectroscopy. Optical properties of Au clusters have received considerable attention, including studies[4a] of naked clusters in gas, polymer, and solvent phases, as well as for MPC solutions[28] and chemisorbed layers.[29] Very small clusters exhibit a strong UV absorption feature which decays approximately exponentially into the visible,[4d] with a superimposed broad band at ∼500 nm (surface plasmon, SP band[4a]) that decreases in intensity and energy with decreasing gold cluster size.[4a,7k] The SP of Au clusters is also sensitive to the surrounding medium, such as interactions[4b] with a optical dielectric of the solvent.

Figure 7 shows UV/vis spectra of hexane solutions of dodecanethiolate-protected Au clusters as a function of their core size. Consistent with a recent study of monodisperse materials,[7k] the SP band intensity decreases dramatically with decreasing cluster size and is undetectable (Figure 7a) for the smallest cluster (−78°,2X,sd). We interpret loss of the SP band as an indication of the onset of quantum size effects (i.e., the loss of bulk character for the smallest Au core).

The next smallest cluster (Figure 7b) does exhibit a peak near the expected SP band wavelength, but very weakly; a second derivative spectrum places this feature at ∼518 nm. The other examples in Figure 7 show that the SP intensity increases with cluster size up to a diameter of ∼4.4 nm (preparation RT,1/8X,fd). These MPCs thus follow the general core size−intensity trend reported[4a] for naked clusters.

The observed SP band energies are, however, independent (± 2 nm) of cluster size (observation uncertainty is greatest for the smaller clusters), which differs from the behavior[4a] of nonligated (naked) metal clusters and which we attribute to the presence of the alkanethiolate ligands. The SP band behavior was further investigated by varying the refractive index of the solvent (hexane, $n_d^{20} = 1.3750$, tetrahydrofuran, $n_d^{20} = 1.4070$, and benzene, $n_d^{20} = 1.5010$). A similar range of refractive indices produces[4b] a 10-nm shift in the SP band energy of colloidal Au. In contrast, the SP band energy of the alkanethiolate-protected cluster is unchanged (at 518 nm, for both the 0°,2X,sd and RT,1/4X,fd clusters) in these solvents; that is, the optical dielectric of the ligand shell, and not that of the solvent, dominates the Au cluster dielectric environment. To examine whether a closer approach of the solvent dielectric could effect a change, clusters were prepared (RT,1/4X,fd protocol) using shorter (butanethiolate and octanethiolate) protecting ligands. The SP band energy was again unchanged (518 nm) and independent of solvent. This interesting phenomenon calls for further experiments using ligands with different refractive indices (e.g., benzylthiolate) and using charged clusters.

Correlation of Monolayer Properties with Core Size: From 3D- to 2D-SAMs. The relationship of monolayer structure and reactivity to the size of the underlying core has seen little scrutiny for MPCs. We have explored this specific question with four techniques: IR spectroscopy (dropcast films and in KBr pellet), DSC, contact angle measurements, and MS of the thermally desorbed organic fragments.

It is important to recall[6c] the two structural motifs on which structural and reactivity differences between monolayers of the same alkanethiolate in a 3D-SAM *versus* a 2D-SAM can be based: (a) a 3D-SAM has a greater concentration of classically defined surface defect sites and (b) a high radius of curvature. The former factor leads to a large coverage of alkanethiolates on the Au surface (%coverage; Tables 2 and 3), and the latter means that chain density changes substantially over the length of an alkyl chain. For example, on a 2.4 nm (diameter) Au core protected by fully extended octanethiolate ligands, the methyl group density is one-fourth that of the Au-S groups at the core surface, with a resulting potential for enhanced mobility of the outermost chain region and/or for lateral chain folding (i.e., large tilt angle). Evidence for such effects has been seen with DOSY[6a] and electrochemical techniques,[6b] in which the measured hydrodynamic cluster radius is less than the sum of the core radius and fully extended alkanethiolate chain length.

Infrared Spectroscopy. Vibrational spectroscopy is a powerful method for understanding alkyl chain orientations in self-assembled monolayers.[6c,7c,30] The C−H stretching and bending vibrations,[31] and C−C and C−S stretching vibrations[32] reliably probe for *gauche* C−C bonds throughout the monolayer. Intensive studies of 2D-SAMs show that the chains are typically in an all-*trans* zigzag configuration.[30] For dropcast (solid-state) films of 3D-SAM protected clusters, at temperatures lower

(28) (a) Kreibig, U.; Fauth, K.; Granquist, C.-G.; Schmid *Z. Phys. Chem.* **1990**, *169*, 11−28. (b) Benfield, R. E.; Creighton, J. A.; Eadon, D. G.; Schmid, G. *Z. Phys. D* **1989**, *12*, 533−536. (c) Kreibig, U.; Fauth, K.; Quinten, M.; Schönauer, D. *Z. Phys. D* **1989**, *12*, 505−514. (d) Fauth, K.; Kreibig, U.; Schmid, G. *Z. Phys. D* **1989**, *12*, 515−520. (e) Kreibig, U. *Sol. State Commun.* **1978**, *28*, 767−769.

(29) (a) Grabar, K. C.; Freeman, R. G.; Hommer, M. B.; Natan, M. J. *Anal. Chem.* **1995**, *67*, 735−743. (b) Freeman, R. G.; Grabar, K. C.; Allison, K. J.; Bright, R. M.; Davis, J. A.; Guthrie, A. P.; Hommer, M. B.; Jackson, M. A.; Smith, P. C.; Walter, D. G.; Natan, M. J. *Science* **1995**, *267*, 1629−1632. (c) Chumanov, G.; Sokolov, K.; Gregory, B. W.; Cotton, T. M. *J. Phys. Chem.* **1995**, *99*, 9466−9471.

(30) (a) Nuzzo, R. G.; Fusco, F. A.; Allara, D. L. *J. Am. Chem. Soc.* **1987**, *109*, 2358−2368. (b) Nuzzo, R. G.; Dubois, L. H.; Allara, D. L. *J. Am. Chem. Soc.* **1990**, *112*, 558−569. (c) Porter, M. D.; Bright, T. B.; Allara, D. L.; Chidsey, C. E. D. *J. Am. Chem. Soc.* **1987**, *109*, 3559−3568.

(31) (a) Snyder, R. G; Strauss, H. L.; Elliger, C. A. *J. Phys. Chem.* **1982**, *86*, 5145−5150. (b) Snyder, R. G.; Maroncelli, M.; Strauss, H. L.; Hallmark, V. M. *J. Phys. Chem.* **1986**, *90*, 5623−5630.

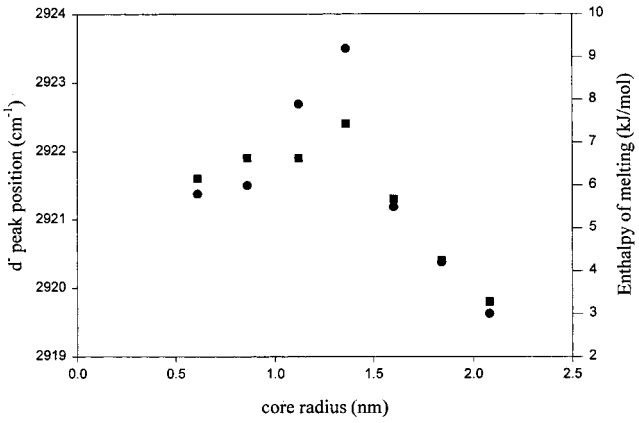

Figure 8. Plot of the d^- peak position (■), which tracks the amount of *gauche* defects in the ligand shell, and the enthalpy of melting (●) as a function of the radius of the dodecanethiolate-protected Au cluster cores.

than the phase transition (*vide infra*), the methylene chain conformations are also mostly all-*trans* zigzag,[6c,7c] but *gauche* defect concentrations at both chain endings are significant (5−25%). This defect concentration increases with increasing temperature (with a phase transition related to alkyl chain melting), decreases with increasing pressure, and increases (for outer chain-end defects) with chain length. The similarity of the bulk (zig-zag) structure to the 2D-SAMs suggests that information about the defects in the 3D-SAMs may be applicable to both systems.

We use the C−H stretching region as a diagnostic of methylene chain ordering. For crystalline polyethylene (low concentration of *gauche* defects), the symmetric (d^+) and antisymmetric (d^-) methylene stretching vibrations lie at 2850 and 2920 cm^{-1}, respectively.[31] Similar values are seen for 2-D SAMs (chains longer than C6),[30] higher ones for liquid alkanes,[31] and smaller ones for highly crystalline long chain (C_{20} or greater) alkanes.[31] For dropcast films of cluster compounds, an unexpected trend emerged [Figure 8 (■)]; that is, the *gauche* defect population does not change monotonically with core size but passes through a maximum at ∼2.8 nm diameter. This curious trend is mirrored by melting enthalpies from DSC studies (*vide infra*) so we defer discussion of it to the next section.

Based on the diagnostic that highly ordered all-*trans* zigzag methylene groups in a 2D-SAM give a d^- stretch at 2920 cm^{-1}, Figure 8 (■) indicates that dodecanethiolate monolayers on a large core [e.g., (RT,1/6X,fd), ∼4.4 nm diameter] have undergone a transition from a 3D-SAM to a 2D-SAM. Assuming a truncated octahedral shape, the estimated maximum defect density of the (RT,1/6X,fd) material is ∼21% (Tables 2 and 3), so large terrace-like regions are present, which should contribute to ordered monolayer packing arrangements. The large cluster also has an average monolayer coverage of 34% (Table 3), a value intriquingly close to that observed[9a] for a 2D-SAM. Further, the texture of samples of this and larger clusters is a free-flowing powder, whereas smaller clusters have either a gummy or waxy consistancy, properties consistent with the crystallinity inferred from the IR spectroscopic measurements. Even so, the presence of such a strongly ordered dodecanethiolate monolayer on a small cluster particle is surprising and may not be a property of an isolated cluster molecule. Interactions beween cluster molecules in the solid cluster films could be important in stabilizing the all-*trans* configuration; solution-phase spectra, which will be reported in a future manuscript,[6h] support this supposition.

Defects at the Au/organic interface are recognized through the C−S stretching vibration ν(C−S), which appears at ∼720 cm^{-1} for an adjacent *trans* C−C bond and at ∼640 cm^{-1} for an adjacent *gauche* (defect) C−C.[6c,32] The relative intensity of these bands measures the relative abundance of near-surface defects.[33] We found that the 640 cm^{-1} *gauche* band was undetectable (i.e., this conformation was present ∼<10% of the population) for the smallest cluster and for clusters >∼3.6 nm diameter, but was weakly present for the midsize clusters. The available evidence[32b] for 2D-SAMs indicates that rougher Au surfaces provoke more near-surface defects. On the cluster molecules, the absence of the ν(C−S) defect band may signal uniformity in the surface binding sites. On the smallest cluster core (−78°,2X,sd), the gold sites are nearly all classically defined defect sites, whereas the largest cluster cores present more nearly all terrace sites. It is only in the midrange of cluster sizes that binding site heterogeneity is sufficient to be detected using ν(C−S).

The aforementioned observations were for dropcast films. Pressing a cluster/KBr mixture into a pellet at 20 000 psi produced more highly ordered materials;[6c] in further experiments, the pressure induced ordering was found to persist even above the melting temperature. For example, the IR spectrum of a pressed pellet of the (90°,2X,sd) cluster is invariant at 25 °C, even after 250 h. Under high pressures, the alkyl chains may interdigitate in a manner forcing out *gauche* defects, and thereafter, the rigid, surrounding KBr lattice inhibits motions that would relax the pressure-induced order. Similar ordering has been observed in polyethylene, but with considerably shorter persistence timescales.[34]

Differential Scanning Calorimetry. Melting transition temperatures and associated heats of enthalpy for alkanethiolate-protected Au clusters[6a,7c] increase with increasing chain length. The melting transitions, which are absent for chains shorter than dodecanethiolate,[35] are presumed to reflect formation of crystalline alkanethiolate domains on cluster surfaces and/or their interdigitation with domains of adjacent clusters. Temperature-dependent IR studies reveal that *trans*-ordering increases in the same cooling temperature region where enthalpic transitions are detected.[7c] Weak melting transitions have also been detected in 2D-SAMs.[36]

Figure 9 shows DSC cooling curves for C12-protected Au clusters over a range of core sizes. (Although some hysteresis occurs between heating and cooling curves, they are quite reproducible and reversible.) The data reveal that the phase transition temperature (∼0 °C) is independent of core size, but the melting enthalpy [normalized to mass of alkanethiolate ligand in the DSC sample; Figure 8 (●)] passes through a maximum that closely mirrors

(32) (a) Hayashi, M.; Shiro, Y.; Murata, H. *Bull. Chem. Soc. Jpn.* **1966**, *39*, 112−117. (b) Bryant, M. A.; Pemberton, J. E. *J. Am. Chem. Soc.* **1991**, *113*, 8284−8293.

(33) The CH_2 rocking vibration (P_x) is also found at ∼720 cm^{-1}; however, the relative intensity of this vibration should be the same for all of the clusters (because the methylene chain length is invariant). Thus, the ratio of $\nu(C-S)_G$:[$\nu(C-S)_T + P_x$] can be compared between each spectrum to obtain relative concentrations of near surface C−C *gauche* defects.

(34) Ito, T. In *High Pressure Science and Technology, Sixth AIRAPT Conference*, Timmerhaus, K. D.; Barber, M. S., Eds.; Plenum: New York, 1977; Vol. 1, pp 482−490.

(35) Both studies reported a DSC trace for a dodecanethiolate protected cluster whose average core size was approximately that of the 314 atom truncated octahedron.

(36) (a) Badia, A.; Back, R.; Lennox, R. B. *Angew. Chem. Int. Ed. Engl.* **1994**, *33*, 2332−2335. (b) Fenter, P.; Eisenberger, P.; Liang, K. S. *Phys. Rev. Lett.* **1993**, *70*, 2447−2450.

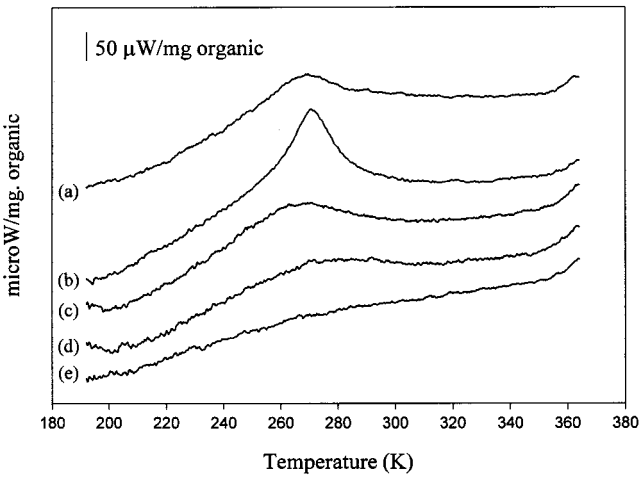

Figure 9. Differential scanning calorimetric traces (cooling curve) of solid-state samples of dodecanethiolate-protected Au cluster compounds: (a) (−78°,2X,sd); (b) (90°,2X,sd); (c) (RT, 1/3X,fd); (d) (RT,1/4X,fd); (e) (RT,1/6X,fd).

that seen for methylene chain ordering [Figure 8 (■); note, the IR measurements were taken at room temperature; i.e., above the melting temperature]. This correspondence suggests that, in part, the melting enthalpy is associated with the energetics of *gauche*/*trans* transitions. Finally, the very small enthalpy for the largest clusters is jointly consistent with assignment to *gauche*/*trans* transitions and the more 2D-SAM-like ordering indicated by the IR results.

The (90°,2X,sd) preparation exhibits both the largest melting enthalpy and the highest number of *gauche* defects. It is pertinent to recall[23] that this cluster may be covered by only a partial monolayer of alkanethiolate ligands. The implication is that although chain ordering on this material can occur at temperatures below the DSC transition, in the melted state the extra space available in the incomplete monolayer leads to a higher level of disorder.

Contact Angle Measurements. The contact angles of water droplets on alkanethiolate 2D-SAMs are linked[37] to the surface energy of the interface between water and the monolayer. Thus, hydrophilic ω-functionalization of the alkanethiolate produces low contact angles and hydrophobic chain termini lead to high contact angles. Contact angles are of interest for the 3D-SAMs because they probe the degree to which the high radius of cluster surface curvature provokes exposure of the methylene chains. The water contact angle on a surface that exposes mostly methylene groups is ∼10° smaller than that for a predominantly methyl group surface.[9b]

Measurement of the water contact angle on a 2D-SAM of dodecanethiol on a Au substrate (a predominantly methyl group surface), under identical conditions as used for thin films of clusters,[38] gave 100.9 ± 1.6°. Water contact angles measured on films of cluster samples were 90.8 to 91.2° for the smallest cores (−78°,2X,sd; 0°,2X,sd; RT,1X,sd), 92.0 to 93.3° for the midsize clusters (RT,1/2X,fd; 1/4X; 1/6X), and as high as 95.3° for the largest clusters (RT,1/8X,fd; 1/10X). All of these values are smaller than that for the 2D-SAM, which is consistent with exposure of methylene segments on the alkanethiolate chain, even on the largest clusters. That the contact angles are smaller for smaller core sizes is also consistent with their higher surface curvature, which should provoke enhanced surface exposure of methylene chain segments.

Surface roughness was considered as a possible source of the variations in contact angles seen for the cluster samples because for contact angles >90°, surface roughness can increase the observed contact angle.[38b] We discount this explanation because cluster films exhibit no obvious change in reflectivity for different core sizes and, in light of the good measurement reproducibility (±1.5° or less), there is also no obvious reason that surface roughness would track cluster core size, at least on dimensions larger than that of the cluster molecules.

Mass Spectrometry. Temperature-programmed desorption MS (at UHV) has been previously applied to small alkanethiolate monolayers on flat gold surfaces. Au(111) coated with methylthiolate (formed from chemisorption of methyldisulfide) decomposes at 180 °C to methyldisulfide.[30a] On Au(110), an ethanethiolate monolayer decomposed not to ethyldisulfide but to ethanethiol at ∼230 °C.[39a] Finally, a hexadecanethiolate monolayer on Au(111) decomposes at 300 °C, although only the desorption of H_2 was reported ($m/e = 2$).[39b]

Figure 10a shows the evolution of total ion current and the *402 m/z* base peak (dodecyl disulfide, $C_{24}H_{50}S_2$) during thermolysis of the (RT,1/4X,fd) Au cluster. Notably, most of the ion current is the 402 ion, which appears over a very narrow temperature range (240−246 °C).[40] The desorption maximizes at 245.7 °C, a temperature compatible with the literature just noted. The plot in Figure 10a is typical, but a few desorption profiles gave multiple peaks clustered around a central desorption temperature.

Spectra averaged over the desorption peak of Figure 10a gave Figure 10b. The base peak at $m/z = 402$ corresponds to the disulfide ($C_{24}H_{50}S_2$) and the peak at $m/z = 201$ is the monomeric unit $C_{12}H_{25}S$. Other sulfur-containing ions in the spectrum include m/z 202 ($C_{12}H_{26}S$), m/z 234 ($C_{12}H_{26}S_2$),[41] and m/z 434 from $C_{24}H_{50}S_3$. The structure and genesis of the latter ion (m/z 434) and another minor peak at higher mass corresponding to $C_{36}H_{74}S_4$ will be the focus of further studies.

Product ion scans (metastable dissociation) of the peak at m/z 402 were obtained for several Au clusters. Figure 10c shows a representative MS/MS spectrum; in this case, for the (−78°,2X,sd) Au cluster. The product ions at m/z 234 ($C_{12}H_{26}S_2$) and m/z 201 ($C_{12}H_{25}S$) result from dissociation of the $C_{24}H_{50}S_2$ disulfide (m/z 402); the difference in the m/z 201/234 ratio in this spectrum compared with the mass spectrum (Figure 10b) is reasonable given that m/z 201 is formed by simple bond cleavage whereas m/z 234 is a rearrangement product. This and other data indicate that the disulfide neutral is formed prior to ionization to $m/z = 402$. Interestingly, Au(111) surfaces have been shown to form disulfides from thiolate monolayers,[30a] whereas Au(110) surfaces give the alkanethiol from the same type of monolayer.[39a] Such a

(37) (a) Folkers, J. P.; Gorman, C. B.; Laibinis, P. E.; Buchholz, S.; Whitesides, G. M.; Nuzzo, R. G. *Langmuir* **1995**, *11*, 813−824, and references therein. (b) Calistri-Yeh, M.; Kramer, E. J.; Sharma, R.; Zhao, W.; Rafailovich, M. H.; Sokolov, J.; Brock, J. D. *Langmuir* **1996**, *12*, 2747−2755. (c) Woodward, J. T.; Ulman, A.; Schwartz, D. K. *Langmuir* **1996**, *12*, 3626−3629.

(38) (a) Harris, J. E. M.A. Thesis, University of North Carolina, Chapel Hill, NC, 1996. (b) Bain, C. D.; Troughton, E. B.; Tao, Y.-T.; Evall, J.; Whitesides, G. M.; Nuzzo, R. G. *J. Am. Chem. Soc.* **1989**, *111*, 321−335.

(39) (a) Jaffey, D. M.; Madix, R. J. *Surf. Sci.* **1994**, *311*, 159−171. (b) Nuzzo, R. G.; Zegarski, B. R.; Dubois, L. H. *J. Am. Chem. Soc.* **1987**, *109*, 733−740.

(40) When the sample is inserted and the temperature immediately raised to 200 °C, the total ion and disulfide ion currents are very broad peaks (30−40 °C). This result may be due to physisorbed or weakly adsorbed disulfides. Holding the sample at 50 °C for 4 min effectively eliminates this type of desorption feature. Further studies will examine this phenomenon.

(41) Analysis of the isotope pattern verified this ion as opposed to oxygen-containing products, such as $C_{12}H_{26}O_2S$.

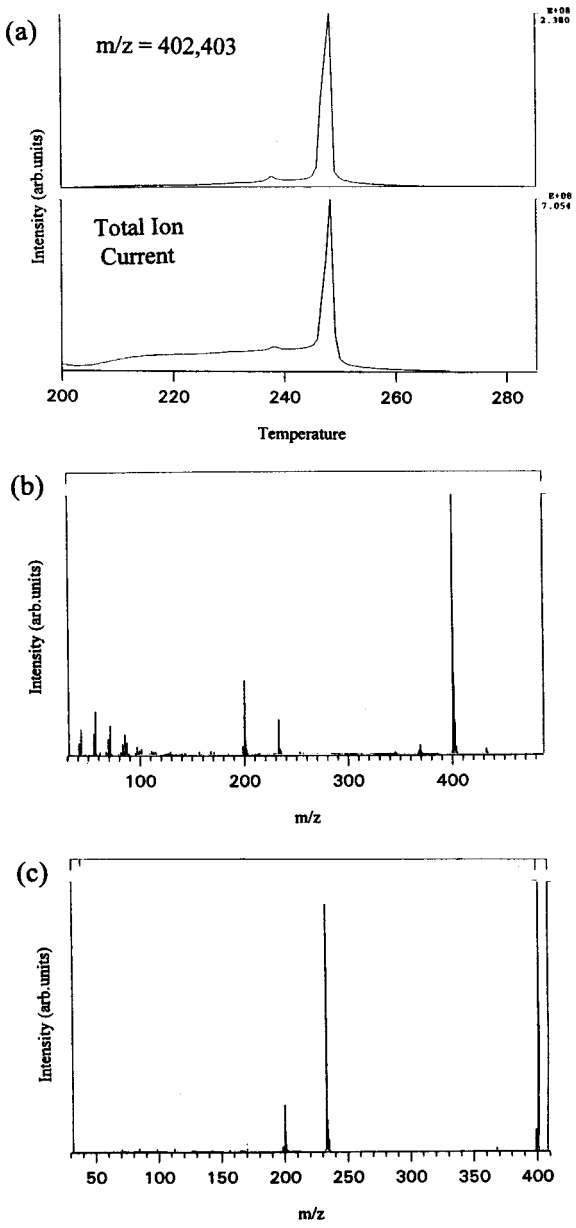

Figure 10. (a) Total ion current and the base peak in the mass spectrum, m/z of 402 (dodecyl disulfide, $C_{24}H_{50}S_2$), versus temperature for the (RT,1/4X,fd) Au cluster. (b) Mass spectrum obtained by averaging scans 84−89 (T = 240−246 °C) in Figure 10a. (c) An MS/MS spectrum (selected for m/z 402) of the major desorption feature during the thermolysis of the (−78°,2X,sd) Au cluster.

comparison may indicate that the cluster Au surface consists mostly of Au(111)-like facets. However, it should be pointed out that such an analysis depends on whether the disulfide forms via reductive elimination or radical recombination after desorption; based on our present data, the distinction between these two mechanisms is not clear.

A plot of desorption temperature versus Au core size suggests a very weak trend toward lower desorption temperature as the core diameter increases. For example, the sharp desorption feature for the (−78°,2X,sd), (RT, 1/4X,fd), and (RT,1/12X,fd) clusters appears at 249, 246, and 236 °C, respectively, suggesting that the monolayer becomes more stable at smaller core sizes. This result might be expected because XPS indicates that the smallest cluster may have a slightly more polarized (RS^-Au^+) bond. There are exceptions, however, to this trend; most notably, the (90°,2X,sd) preparation decomposes at 235 °C. However, that material (vide supra) likely contains only a partial monolayer,[23] so chain/chain interactions may be helping to stabilize the other monolayers.

Summary

Manipulation of reaction conditions, notably the thiol: Au ratio, the reduction temperature, and the rate of reductant addition, yields alkanethiolate-protected Au clusters with a range of core sizes, dispersity levels, and monolayer coverages. The combined results from ^{1}H NMR line broadening, SAXS, HR TEM, and TGA establish that the smallest and largest clusters have average diameters of 1.5 and 5.2 nm, respectively. This range corresponds to cores containing ∼110 to 4800 (average) Au atoms and from 53 to nearly 520 alkanethiolate chains. In each cluster preparation, moderate size dispersity was seen, with an average standard deviation of ∼10−20% about the average core size. Accordingly, the measured properties should not be taken as perfectly peculiar to a particular cluster core size.

That being said, the resulting chemical and physical properties of these materials were correlated with average core size. For example, the electronic properties of the Au core appear to be consistently metallic over the entire range of core sizes, although it is also evident that a change from a nano-sized segment of bulk metal to that of a "quantum-sized" metal cluster begins near a core size of ∼200 atoms. (a) The XPS spectrum changes only slightly as the core size decreases, slightly shifting towards the values seen for the $[AuSR]_n$ polymer; (b) the UV/vis spectrum displayed a surface plasmon band characteristic of the bulk metal at that core size, but which disappeared for smaller cores.

The transition between a 2D-SAM and a 3D-SAM for a dodecanethiolate monolayer was also investigated. The chain conformations, as probed by IR spectroscopy, are substantially more ordered for the largest particles. Using this criteria, a core diameter of ∼4.4 nm links the two different dimensional systems (other chainlengths will likely exhibit somewhat different transition sizes). Results of DSC and contact angle measurements are consistent with this assignment. Although the radius of curvature is still high for a 4.4 nm cluster, the predominance of flat surfaces over edges and corners seems to allow a core of this size to reasonably mimic a 2D-surface (high crystallinity, small phase transitions, and an exposed CH_3 surface).

The other substantial result to emerge from this study is that thermolysis of the clusters produces only the corresponding disulfide. The absence of thiol is evidence that the chemisorbed ligand consists of an alkanethiolate (not thiol) fragment. The bulk of the disulfide desorbs over a narrow temperature range (3−4 °C); the implications of this behavior will be presented shortly.

Acknowledgment. This work was supported by grants from the National Science Foundation and the Department of Energy. The HRTEM work was sponsored by the Division of Materials Sciences, U.S. Department of Energy, under contract DE-AC05-96OR22464 with Lockheed Martin Energy Research Corp., and through the SHaRE Program under contract DE-AC05-76OR00033 with Oak Ridge Associated Universities. The SAXS work at ORNL is supported by the Division of Materials Sciences, U.S. Department of Energy, under contract with Martin Marietta Energy Systems Inc. The work of CJZ and MDP was supported by the Office of Basic Energy Sciences, Chemical Sciences Division, and by the Mi-

croanalytical Instrumentation Center of Iowa State University; J. Anderegg's assistance with the XPS measurements is also acknowledged. Access to the TGA equipment was provided by Professor J. DeSimone of UNC. JEH acknowledges the receipt of a NSF pre-doctoral fellowship. The authors gratefully acknowledge Dr. Wei Ou and Dr. Richard Linton of UNC for preliminary XPS experiments, Dr. H. Masui of UNC, Professor Linda Reven (McGill University and Prof. Robert Whetten (Ga. Tech.) for insightful discussions on the project, and Dr. E. Pascal for assistance with the HRTEM data analysis.

Supporting Information Available: Further experimental details (3 pages). Ordering and/or access information is given on any current masthead page.

LA970588W